SUCLG1 promotes aerobic respiration and progression in plexiform neurofibroma

ZIFU ZHOU[1], QINGFENG LI[2] and RAN HUO[1,3,4]

[1]Department of Burn and Plastic Surgery, Shandong Provincial Hospital, Cheeloo College of Medicine, Shandong University, Jinan, Shandong 250021, P.R. China; [2]Department of Plastic and Reconstructive Surgery, Shanghai Ninth People's Hospital, Shanghai Jiao Tong University School of Medicine, Shanghai 200011, P.R. China; [3]Department of Burn and Plastic Surgery, Shandong Provincial Hospital Affiliated to Shandong First Medical University, Jinan 250021, P.R. China; [4]Medical Science and Technology Innovation Center, Shandong First Medical University and Shandong Academy of Medical Sciences, Taian, Shandong 271000, P.R. China

Received July 31, 2024; Accepted November 21, 2024

DOI: 10.3892/ijo.2024.5716

Abstract. Plexiform neurofibromas (PNFs) are benign tumors that affect 20-50% of patients with type I neurofibromatosis (NF1). PNF carries a risk of malignancy. There is no effective cure for PNF. Its onset may be associated with genetic and metabolic abnormalities, but the exact mechanisms remain unclear. Succinate-CoA ligase GDP/ADP-Forming Subunit α (SUCLG1), a catalytic enzyme in the tricarboxylic acid cycle, is highly expressed in PNF. The present study aimed to explore the role of SUCLG1 in function and metabolism of PNF cells. SUCLG1 expression was verified using western blotting and immunofluorescence. After inducing SUCLG1 knockdown and overexpression, functional changes in PNF cells were assessed, as well as effects of SUCLG1 on cell respiration and glucose metabolism. Quantitative PCR, WB, electron microscopy and Flow cytometry demonstrated that SUCLG1 enhanced mitochondrial quality and promoted mitochondrial fusion, thereby driving proliferation and migration of tumor cells, inhibiting apoptosis and altering the cell cycle. A Seahorse assay showed that elevated SUCLG1 expression enhanced cell aerobic respiration without affecting the glycolytic process. This suggests that SUCLG1 upregulation in PNF does not trigger the Warburg effect associated with malignant tumors. This study also demonstrated the positive regulation of cellular function by promoting the expression level of the *SLC25A1* gene when SUCLG1 expression was elevated. In conclusion, SUCLG1 altered the mechanism of mitochondrial quality control to enhance cell aerobic respiration, thereby driving the pathogenesis of PNF. Thus, SUCLG1 can serve as a potential target in future therapeutic strategies.

Correspondence to: Professor Ran Huo, Department of Burn and Plastic Surgery, Shandong Provincial Hospital, Cheeloo College of Medicine, Shandong University, 324 Jing Wu Road, Jinan, Shandong 250021, P.R. China
E-mail: huoran@email.sdu.edu.cn

Professor Qingfeng Li, Department of Plastic and Reconstructive Surgery, Shanghai Ninth People's Hospital, Shanghai Jiao Tong University School of Medicine, 639 Zhizaoju Road, Shanghai 200011, P.R. China
E-mail: dr.liqingfeng@shsmu.edu.cn

Key words: plexiform neurofibroma, mitochondria, aerobic respiration, neurofibromatosis type 1, tricarboxylic acid cycle

Introduction

Neurofibromatosis type 1 (NF1) is a rare autosomal dominant disorder caused by mutations in *NF1* gene, with a global incidence of ~1 in 3,000 live births (1). Patients are at risk of developing benign and malignant tumors throughout their lives, and typical symptoms include plexiform neurofibroma (PNF), which occurs in 20-50% of patients with NF1 mutation (2-4). Patients often present with painful, oversized masses that interfere with function in early childhood that rapidly progress during childhood and adolescence (5). PNF tumors may spread extensively and invade surrounding tissue, causing severe physical defects and functional impairment, resulting in high rates of disability and malformation. As the patient ages, risk of the tumors transforming into malignant peripheral nerve sheath tumors (MPNSTs) increases, posing a threat to the patient life and health (4). However, current clinical treatments for PNF are limited because the tumors grow along nerves, and some types are poorly circumscribed from surrounding tissue, frequently causing difficulties in surgical resection (6). Furthermore, the indications (such as patient age and tumor progression) for surgery are often unclear and risky and the tumors are prone to recurrence (6). In 2020, selumetinib, a mitogen-activated protein kinase inhibitor, became the first effective targeted therapy approved for PNF and is currently the preferred treatment option for pediatric patients with inoperable PNF (7,8). However, issues remain, including the 30% rate of primary drug resistance, secondary drug resistance following long-term drug use and lack of treatment options in adulthood (7,8). Therefore, development of novel targeted drugs is still urgently needed.

Mass spectrometry and non-targeted metabolomics analysis found that SUCLG1 and citric acid (CA) in the catalytic

enzyme pathway of the tricarboxylic acid cycle (TCA) are highly expressed in PNF (9). SUCLG1 is responsible for converting succinyl-CoA into succinate (10). Mutations in SUCLG1 are implicated in metabolic disorders, fatal infantile lactic acidosis and mitochondrial DNA depletion (10,11). In a recent study, SUCLG1 was found to be associated with leukemia progression (12). To the best of our knowledge, however, no other tumors have been studied in relation to SUCLG1. CA is an important signaling molecule in cell metabolism. CA is synthesized by citrate synthase (CS) and transported from the mitochondria to the cytoplasm via a CA carrier (SLC25A1). It is then broken down by ATP citrate lyase (ACLY) into oxaloacetate and acetyl CoA, which are used to synthesize pro-inflammatory factors such as reactive oxygen species (ROS) and nitric oxide (NO), as well as lipids (13,14). To the best of our knowledge, neither the SUCLG1 gene nor changes in tumor metabolism have been studied in relation to PNF.

The present study aimed to examine the role of SUCLG1 in the function and metabolism of PNF cells and explore its potential as an effective target for treatment of PNF.

Materials and methods

Tissue collection and cell culture. A total of three pairs of PNF and normal human skin tissue and four pairs of serum samples were obtained from the Department of Plastic Surgery, Shandong Provincial Hospital, Jinan, Shandong, China with informed written consent and approval from the Human Research Ethics Review Committee of Shandong Provincial Hospital (approval no. SWYX2024-556). The samples were collected from four patients (three male, one female; mean age, 18.25±3.40 years) from April 2021 to April 2022. The inclusion criteria were as follows: i) Patients with PNF; ii) the lesion involved skin tissue and iii) no other disease. According to the inclusion criteria, the lesions invaded the skin tissue; therefore, normal skin was used as the control group. Demographic characteristics are shown in Table SI. PNF cells (ipNF95.6 and ipNF05.5; American Type Culture Collection; cat. nos. CRL3389 and CRL3387, respectively) were donated by the Department of Plastic Surgery, Shanghai Ninth People's Hospital, Jinan, China. The human Schwann cell (HSC) line was purchased from Zhong Qiao Xin Zhou Biotechnology Co., Ltd. and cultured in HSC immortalization medium (ZMY106; Zhong Qiao Xin Zhou Biotechnology Co., Ltd.) at 37˚C in an atmosphere containing 5% CO_2. PNF cells and 293T cells were cultured in high-glucose DMEM (Gibco; Thermo Fisher Scientific, Inc.) containing 10% FBS (Procell Life Science & Technology Co., Ltd.) and 1% penicillin/streptomycin at 37˚C in an atmosphere containing 5% CO_2.

Proteomics and metabolomics analysis. Proteomics and non-targeted metabolomics analysis were performed with skin tissue and serum samples from patients with PNF and healthy individuals, respectively. Proteomics was performed using conventional high performance liquid chromatography (LC20AD, Shimadzu) for processing samples with a column temperature of 40˚C and a flow rate of 1 ml/min. Instruments used for metabolomics are Mass Spectrometer (Q Exactive™ HF, Thermo Fisher, Germany), chromatograph (Vanquish UHPLC, Thermo Fisher, Germany) and chromatographic column (Hypesil Gold column(C18), Thermo Fisher, USA). Positive and negative ionisation modes were used, the scanning range was 100-1,500 m/z, the Sheath gas flow rate was 35 psi, and the Aux gas heater temp was 350˚C. $P<0.05$ and fold-change (FC)≥1.2 or ≤0.83 in the protein sample and FC ≥2 or ≤0.5 and variable importance in the projection ≥1 in the serum metabolite samples were considered to indicate a statistically significant difference. R1.6.20, VennDiagram package (omicstudio.cn/tool.) was used to visualize data. Kyoto Encyclopedia of Genes and Genomes(KEGG; genome.jp/kegg) pathway was plotted using the OmicStudio (omicstudio.cn/tool.)

Reverse transcription-quantitative (RT-q)PCR. Total RNA of cells was extracted using RNAiso Plus (Takara Bio, Inc.), and cDNAs were reverse-transcribed from 1 μg total RNA using HiScript RT SuperMix for qPCR (Vazyme Biotech Co., Ltd.) at 4˚C for 20 min. DNA of cells was extracted with a DNA Isolation Mini kit (Vazyme Biotech Co., Ltd.). qPCR was performed using SYBR Green Master Mix (Vazyme Biotech Co., Ltd.) on the LightCycler 480 II (Roche Diagnostics). Thermocycling conditions were as follows: Pre-denaturation at 95˚C for 30 sec, followed by 40 cycles at 95˚C for 5 sec and 60˚C for 30 sec and final extension at 95˚C for 15 sec, 60˚C for 60 sec and 95˚C for 15 sec. β-actin was selected as the internal control. $2^{-\Delta\Delta Cq}$ was used to calculate relative expression (14). To measure mtDNA content, we used 1 μg DNA and primers to the Journal Pre-prooD-loop region of the mitochondrial genome. G6PC primers served as genomic DNA control to normalize the mitochondrial to the genomic DNA ratio. The primers are listed in Table SII.

Western blotting (WB). Total protein of cells was extracted using the Minute Total Protein Extraction kit (Invent Biotechnologies, Inc.) or RIPA Lysis Buffer (Beyotime Institute of Biotechnology). Protein concentration was determined using a BCA Protein Assay Kit (Beyotime Institute of Biotechnology). A total of 20 μg/lane protein was separated by 10% SDS-PAGE, proteins were placed in rapid QuickBlock Blocking Buffer for WB (Beyotime Institute of Biotechnology; cat. no. P0252) and blocked for 20 min at 25˚C, then transferred to polyvinylidene fluoride membranes and incubated with primary antibodies at 4˚C overnight. The primary antibodies included β-actin (Proteintech Group, Inc.; 66009-1-I; 1:1,000), α-tubulin (Wuhan Servicebio Technology Co., Ltd.; cat. no. GB15201; 1:2,000), SUCLG1 rabbit mAb (Cell Signaling Technology, Inc.; cat. no. 8071; 1:1,000), CS rabbit pAb (cat. no. A5713; 1:1,000), SLC25A1 Rabbit pAb (cat. no. A24754; 1:5,000), mitofusin-1 (MFN1) rabbit pAb (cat. no. A9880; 1:1,000), MFN2 rabbit mAb (cat. no. A19678; 1:1,000), OPA1 (optic Atrophy Protein 1) rabbit pAb (all ABclonal Biotech Co., Ltd.; cat. no. A9833; 1:4,000) and ACLY rabbit pAb (Proteintech Group, Inc.; cat. no. 15421-1-AP; 1:2,000). Then, the membranes were incubated with HRP-conjugated goat anti-rabbit secondary antibodies (cat. no. SA00001-2; 1:10,000) or anti-mouse secondary antibodies (both Proteintech Group, Inc.; cat. no. SA00001-1; 1:10,000) at 25˚C for 1 h. Enhanced chemiluminescent solution (Sparkjade ECL plus, ED0016-B; Sparkjade) and ChemiDoc Imaging System (Bio-Rad Laboratories, Inc.)

was used to quantify the expression of proteins. ImageJ 1.53e (National Institutes of Health) analyses the greyscale values and performs calculations.

Immunofluorescence staining. Tissues were fixed with 4% polydoxaldehyde at room temperature for 24 h, dip-waxed at ~60˚C for 4.5 h and then embedded in paraffin. The pre-cooled wax blocks were sectioned (thickness, ~3 μm). The slices were placed in the oven at 60˚C for 1 h. Slices were placed in Eco-friendly dewaxing solution I for 10 min-Eco-friendly dewaxing solution II for 10 min-Eco-friendly dewaxing solution III (Wuhan Servicebio Technology Co., Ltd.; cat. no. G1128) for 10 min-anhydrous ethanol I for 5 min-anhydrous ethanol II for 5 min-70% alcohol for 5 min-and washed with distilled water. Sections were placed in citric acid antigen repair solution (pH, 6; Wuhan Servicebio Technology Co., Ltd.; cat. no. G1202), microwaved for 10 min on medium heat, ceased for 5 min, transferred to medium-low heat for 5 min, ceased for 2 min and finally medium-low heat for 5 min, and recovered at room temperature for 30 min. Dewaxed sections were placed in 3% hydrogen peroxide and incubated for 20 min at room temperature , then closed with 3% BSA (Wuhan Servicebio Technology Co., Ltd.; cat. no. GC305010) for 30 min at room temperature. Dewaxed sections were stained with primary antibodies against SUCLG1 (Cell Signaling Technology, Inc.; cat. no. 8071; 1:100) and recombinant anti-160 kDa neurofilament medium antibody (Wuhan Servicebio Technology Co., Ltd.; cat. no. GB15763-100; 1:500) at 4˚C overnight, and then incubated with CY3-labelled goat anti-rabbit and Alexa Fluor 488 labelled goat anti-mouse IgG. (cat. nos. GB21303 and GB25301; both 1:300; both Wuhan Servicebio Technology Co., Ltd) at room temperature in the dark for 50 min, and DAPI stain solution was added at room temperature in the dark for 10 min before fluorescence microscopy (NIKON ECLIPSE C1; Nikon Corporation). Magnification is 50x. Data were analyzed using ImageJ 1.53e (National Institutes of Health, USA).

Knockdown and overexpression (OE) of SUCLG1. Recombinant packaging plasmids (PG-P1-VSVG, PG-P2-REV and PG-P3-RRE) and vector plasmids (lentivirus vector) were prepared by GenePharma Co., Ltd. A total of 1 μg third generation lentiviral packaging system package mix was prepared in the ratio of PG-P1-VSVG:PG-P2-REV:PG-P3-RRE 1:2:3 for the lentiviral plasmid packaging experiments in 60-mm cell culture dishes. RNAi-Mate (GO4001, GenePharma Co., Ltd, Shanghai, China) to co-transfect 293T cells (GenePharma Co., Ltd, Shanghai, China). OE SUCLG1 plasmid backbone was LV5(EF-1a/GFP&Puro) and its sequence was 5'-TTC TCCGAACGTGTCACGT-3'. ShSUCLG1-containing plasmid backbone was LV3(H1/GFP&Puro) and its sequence was 5'-AGATCTGGCACCCTGACTTAT-3'. Sequence of shSUCLG1 negative control was 5'-TTCTCCGAACGT GTCACGT-3'. The multiplicity of infection of both the knockdown and overexpression lentivirus was 100. ipNF05.5 and ipNF95.6 2x10^5 cells were seeded onto six-well plates (Corning, Inc.). After adding short hairpin negative control (shNC) and shSUCLG1 to ipNF05.5 and OE-SUCLG1 and NC to ipNF95.6, the cells were infected for 24 h at 37˚C and then the medium was replaced with a fresh high-glucose DMEM (Gibco; Thermo Fisher Scientific, Inc.) containing 10% FBS (Procell Life Science & Technology Co., Ltd.). Transfection efficiency was assessed based on the expression of green fluorescent protein 72 h after transfection by fluorescence microscopy. Successfully infected cells were immediately subjected to subsequent experiments.

Inhibitor-treated cells. 50 μM of the inhibitor of SLC25A1 (CTPI-2; Cat. No. HY-123986; MedChemExpress) was added to the cells of OE-SUCLG1 group, which were then incubated in a 37˚C incubator for 24 h before subsequent functional experiments.

Cell Counting Kit 8 (CCK-8) assay. ipNF95.6 and ipNF05.5 2x10^3 cells were seeded onto 96-well plates (Corning, Inc.). At 2 h (37˚C after seeding, 10 μl CCK-8 (Wuhan Elabscience Biotechnology Co., Ltd.) was added to each well. The optical density was measured after 2, 12, 24 and 36 h at 450 nm by Multiskan FC Microplate Photometer (Catalog #1410101, Thermo Fisher, USA).

Wound healing assay. A total of 2x10^5 virus-infected cells were seeded onto six-well plates to 90% confluence and scratched. After rinsing the free cells in PBS, the medium was replaced with fresh DMEM without FBS. Cell migration was observed at 0 and 24 h by light microscope. Magnification is 100x. Migration rate was calculated using ImageJ 1.53e (National Institutes of Health) as follows: (Width at 0 h-width at 24 h)/width at 0 h.

Flow cytometry. Virus-infected cells were washed twice with cold PBS and resuspended in 1X Binding Buffer (PE Annexin V Apoptosis Detection kit I; BD Biosciences; cat. no. 559763) at a concentration of 1x10^6 cells/ml, according to the manufacturer's instructions. PE Annexin V and 5 μl 7-AAD were added to stain the cells. After incubation at 25˚C for 15 min in the dark, cell apoptosis was detected via flow cytometry. The sum of early and late apoptotic cells gives the total percentage of apoptotic cells in the sample. When determining cell cycle phase using the Cell Cycle Detection kit (Nanjing KeyGen Biotech Co., Ltd.; cat. no. KGA512), a cell suspension containing 1x10^6 cells/ml was washed with PBS, centrifuged (380 x g, 5 min) at 4˚C and fixed with 70% ethanol at 4˚C overnight. The cells were stained with pre-prepared PI/RNase A Staining Solution (1:9 ratio) at 25˚C for 30 min in the dark before loading into CytoFLEX S (Beckman Coulter, Inc.) for detection. Data were analyzed using FlowJo 10.8.1 (BD Biosciences).

Transmission electron microscopy. After washing with PBS, the virus-infected cells were pre-fixed with 3% glutaraldehyde at 4˚C overnight and re-fixed with 1% osmium tetroxide at 25˚C for 2 h. This was followed by dehydration, infiltration and embedding with Epon-812 (45345, MerckMillipore) at 70˚C overnight. Sections (60-90 nm) were cut using an ultrathin sectioning machine (cat. no. UC7rt; Leica GmbH). The sections were stained with uranyl acetate for 10-15 min at room temperature, then with lead citrate for 1-2 min at

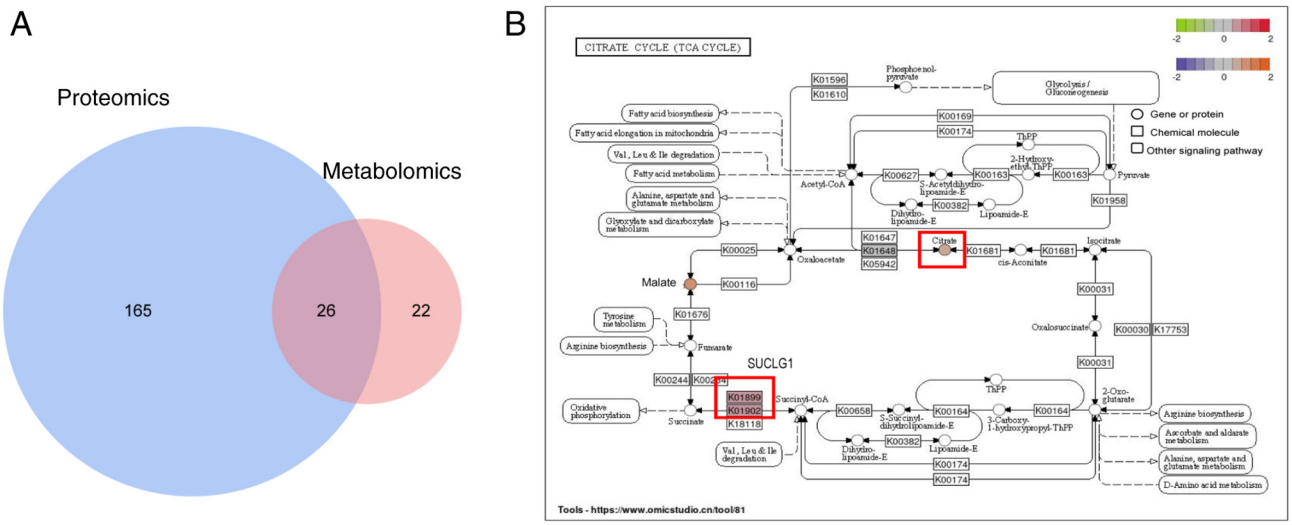

Figure 1. Analysis of proteomics and metabolomics. (A) Distribution of pathways in which differentially expressed proteins and metabolites were enriched. (B) Proteins and metabolites enriched in the TCA. SUCLG1, succinate-CoA ligase GDP/ADP-forming subunit α; K01899, succinate-CoA ligase GDP-forming subunit α; K01902, succinate-CoA ligase ADP-forming subunit α; TCA, tricarboxylic acid cycle.

room temperature. Cells were observed and photographed using a transmission electron microscope (JEOL Ltd.; cat. no. JEM-1400FLASH).

ROS measurement. Complete medium of $1x10^6$ virus-infected cells was centrifuged (860 x g) at 4˚C for 20 min, and the supernatant was collected. ROS ELISA Research kit (Jiangsu ELISA Industry Co., Ltd.; cat. no. MM-1893H2) was used to assess ROS levels by measuring the absorbance of each well at 450 nm, according to the manufacturer's instructions. The concentration of the sample was calculated based on the standard curve.

Determination of metabolite content and activity. A total of $1x10^6$ virus-infected cells was collected, and 1 ml extract solution (Keyybio; cat. no. ADS-W-S002) was added. The cells were disrupted by ultrasonication at low power on an ice bath (3 sec followed by 7 sec; total time, 3 min). After centrifugation (13,680 x g) at 4˚C for 10 min, the supernatant was discarded. CA Content kit (Keyybio; cat. no. ADS-W-S002) was used according to the manufacturer's instructions. After incubation at room temperature for 20 min, absorbance *A* was measured at 470 nm to calculate Δ*A*=*A* blank-*A* measured. Values from the standard curve were used to calculate the CA content. Activity assays were performed using CS (cat. no. MM-63621H2) and ACLY ELISA Research kits (both Keyybio; cat. no. KYY-62138H1), according to the manufacturer's instructions. Absorbance of each well was measured at 450 nm. The standard curve was plotted, and the concentration of the samples was calculated.

Metabolic energy assay. A total of 8 ml of $5x10^4$/ml virus-infected cell suspension was plated on XF96 cell culture plates (Agilent Technologies, Inc.) and cultured at 37˚C overnight. The probe plate was hydrated with XF Calibrant and placed in a non-CO_2 cell culture incubator at 37˚C overnight. On the second day, the probe plate was re-hydrated with sterile water and the detection solution was prepared to wash the cells. The detection solution consisted of 97 ml 103575-100 Seahorse XF DMEM (PH 7.4, Agilent Technologies, Inc.), 1 ml glucose (103577-100, Agilent Technologies, Inc.), 1 ml pyruvate (103578-100, Agilent Technologies, Inc.) and 1 ml glutamine (103579-100, Agilent Technologies, Inc.) Seahorse XF Cell Mito Stress Test kit (cat. no. 103015-100) and Seahorse XF Glycolysis Seahorse XF (both Agilent Technologies, Inc.; cat. no. 103020-100) were used according to the manufacturer's instructions. The Agilent Seahorse XFe96 Analyzer was used to measure oxygen consumption rate and extracellular acidification rate.

Statistical analysis. The data were analyzed using GraphPad Prism 9.4.1 (Dotmatics, Inc.). Data are presented as the mean and standard deviation, after three independent experimental replications. One-way ANOVA and Tukey's post hoc test was performed to evaluate the differences. Paired Student's t test was performed to evaluate the differences between two groups. $P<0.05$ was considered to indicate a statistically significant difference.

Results

Proteomics and metabolomics results. *Proteomic analysis* was performed with the tissues of patients with PNF and healthy individuals, whereas non-targeted metabolomic analysis was performed with serum samples. Table SIII shows differentially expressed proteins measured by mass spectrometry sequencing and metabolites measured by non-targeted sequencing. A total of 26 pathways were enriched (Fig. 1A). Among these 26 pathways, the protein with the highest expression was SUCLG1 (Table SIII). Based on the results of the co-analysis, SUCLG1 affected PNF in the TCA cycling pathway, which targeted CA (Fig. 1B).

Verification of SUCLG1 and CA levels. Immunofluorescence indicated that the levels of SUCLG1 were higher in PNF tumor tissues than in normal skin tissues (Fig. 2A and B). SUCLG1 was distributed along the nerve. WB showed that at a cellular

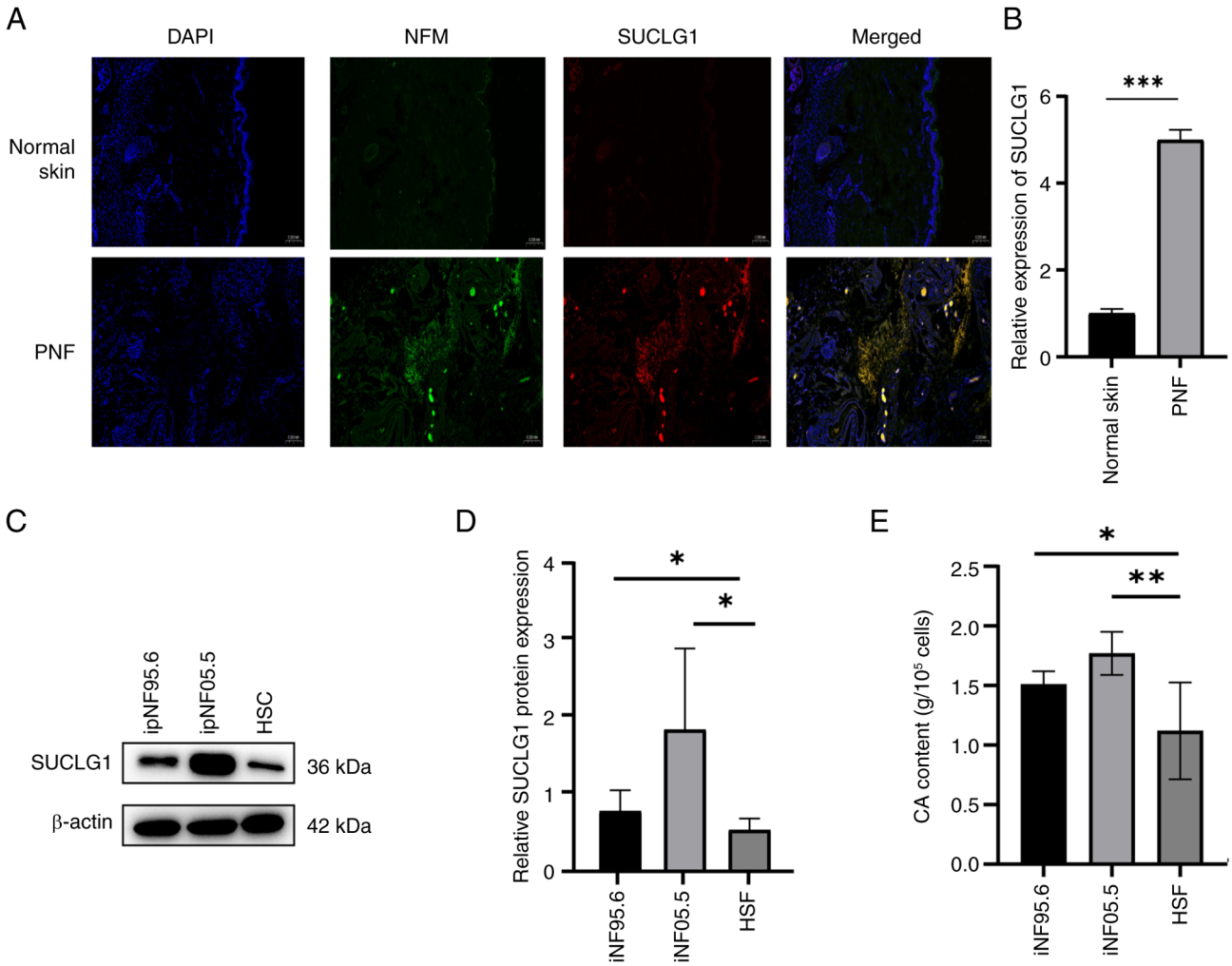

Figure 2. SUCLG1 and CA are highly expressed in PNF. (A) Representative immunofluorescence staining of (B) SUCLG1 expression in normal skin and PNF. Magnification, x50x. (C) Western blotting for (D) SUCLG1 expression in ipNF95.6, ipNF05.5 and HSCs. (E) CA content in ipNF95.6, ipNF05.5 and HSCs. *P<0.05, **P<0.01, ***P<0.001. SUCLG1, succinate-CoA ligase GDP/ADP-forming subunit α; CA, citric acid; PNF, plexiform neurofibroma; HSC, human Schwann cell; NFM, neurofilament medium.

level, expression of SUCLG1 in PNF cells was higher than that in HSC. ipNF05.5 cells showed higher levels of SUCLG1 expression than ipNF95.6 cells (Fig. 2C and D). In addition, the content of CA in PNF cells was higher than that in the cells of normal skin samples (Fig. 2E).

Regulation of PNF cell function by SUCLG1. SUCLG1 knockdown in ipNF05.5 cells and overexpression in ipnF95.6 cells were induced to explore the *in vitro* effects of SUCLG1. Transfection efficiency was verified by fluorescence photography. Knockdown and overexpression efficiency were confirmed by RT-qPCR and WB (Fig. 3A-C). CCK-8 assay indicated that the proliferative capacity of PNF cells decreased following SUCLG1 knockdown and increased upon overexpression (Fig. 3D and E). Similarly, wound healing assay revealed that the migratory ability of PNF cells decreased following SUCLG1 knockdown and increased after SUCLG1 overexpression (Fig. 3F and G). SUCLG1 knockdown resulted in a decrease in the proportion of cells in S phase and a concomitant increase in the proportion of total apoptotic cells (Q2 + Q3; Fig. 3H-K). By contrast, overexpression resulted in an increased proportion of cells in S phase and suppressed the proportion of total apoptotic cells.

Effect of SUCLG1 on intracellular metabolism. To examine the effect of SUCLG1 on intracellular metabolism, the present study used a mitochondrial stress test (Fig. 4A). Basal respiration, ATP production and maximum respiratory rate decreased after SUCLG1 knockdown. However, these parameters also increased following OE, suggesting an improvement in the levels of mitochondrial aerobic respiration (Fig. 4B and C). There no significant differences in glycolysis levels between groups (Fig. 4D and E). This implies that SUCLG1 mainly regulated the level of mitochondrial aerobic respiration in PNF cells and had no effect on the levels of glycolysis.

Effect of SUCLG1 on mitochondrial quality control. To assess mitochondrial changes supporting increased aerobic respiration., RT-qPCR was performed to determine the relative copy number of mtDNA) with respect to the genomic DNA (gDNA) to determine mitochondrial DNA content. Ratio of mtDNA to gDNA increased when SUCLG1 was overexpressed and decreased when SUCLG1 expression was knocked down

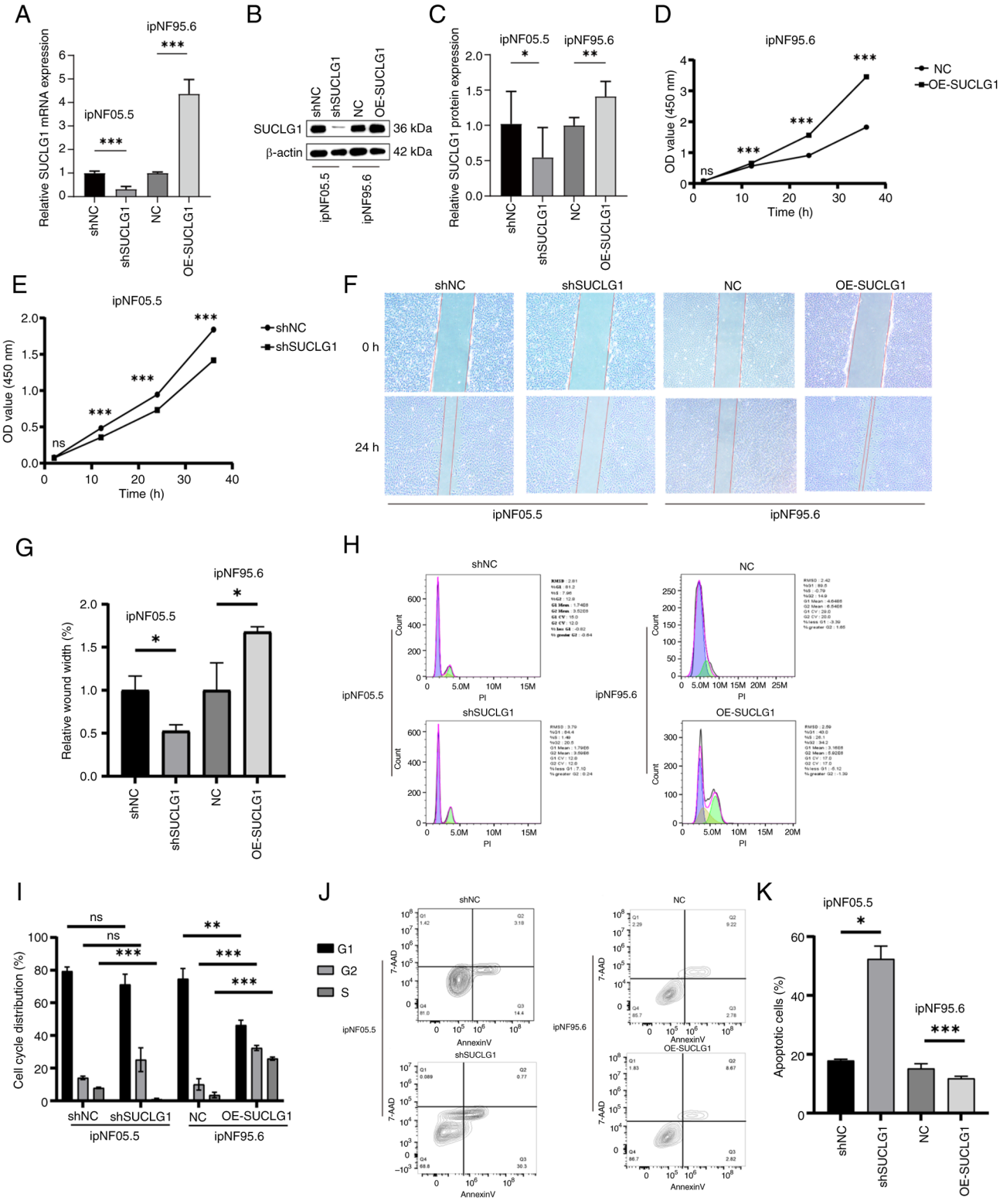

Figure 3. Regulation of PNF cell function by SUCLG1 expression. (A) Reverse transcription-quantitative PCR analysis of SUCLG1 in ipNF05.5 and ipNF95.6 cells after transfection. (B) Western blotting of (C) SUCLG1 expression in ipNF05.5 and ipNF95.6 after transfection. Proliferation of (D) ipNF95.6 and (E) ipNF05.5 cells. (F) Wound healing assay showing, Magnification, x100x. (G) Wound width of PNF cells after transfection. (H) Representative flow cytometry of (I) cell cycle distribution in PNF cells after transfection. (J) Representative flow cytometry of (K) apoptosis in PNF cells after transfection. *P<0.05, **P<0.01, ***P<0.001 vs. 0 h. ns, not significant; PNF, plexiform neurofibroma; SUCLG1, succinate-CoA ligase GDP/ADP-forming subunit α; sh, short hairpin; NC, negative control; OE, overexpression; OD, optical density.

(Fig. 4F). As aerobic respiration may have been regulated by changes in mitochondrial dynamics (16), transmission electron microscopy was performed to evaluate mitochondrial morphology. When SUCLG1 was highly expressed, mitochondria appeared elongated and deformed, which was hypothesized to be a sign of fusion (Fig. 4G). Compared with

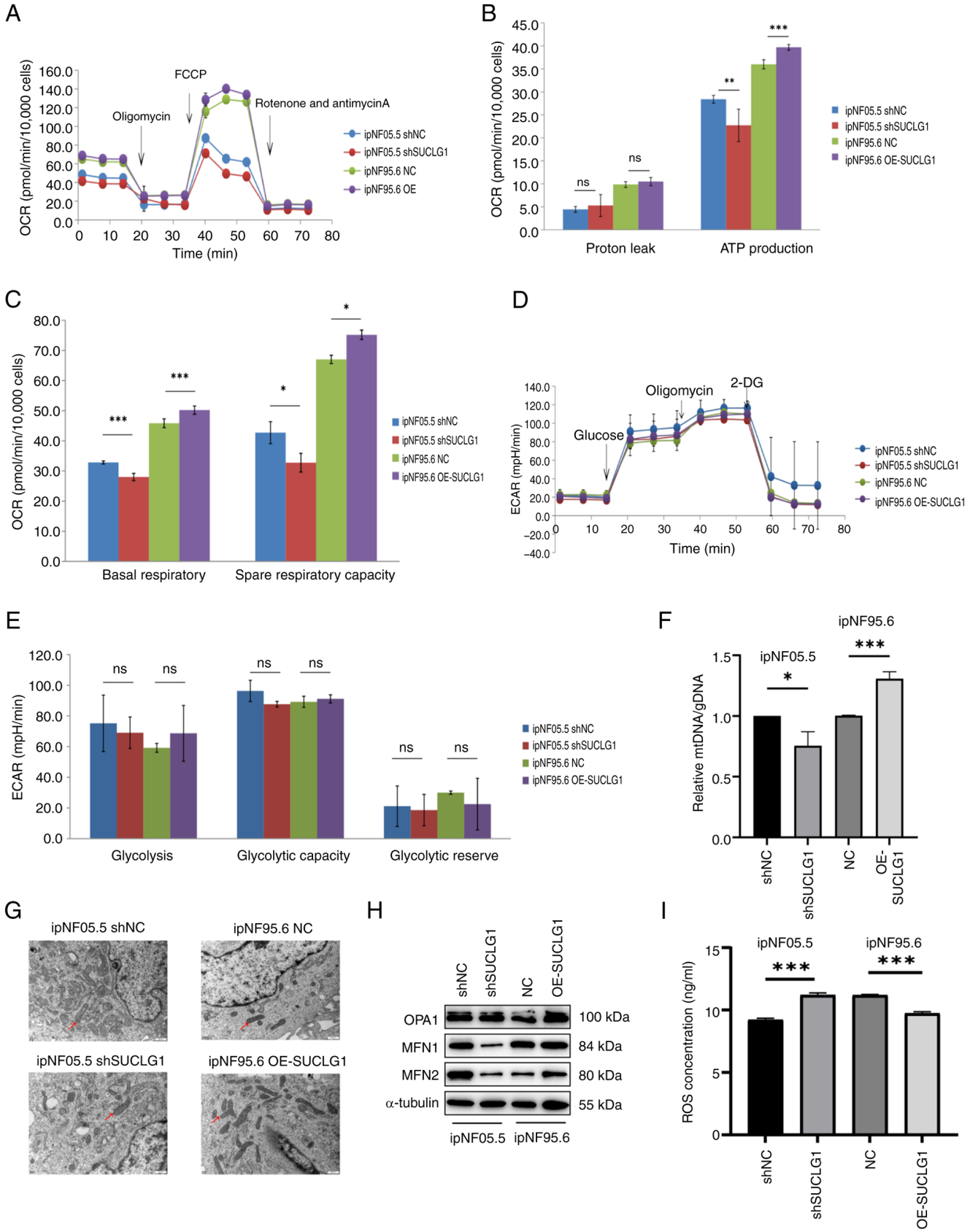

Figure 4. Effect of SUCLG1 on intracellular metabolism and mitochondrial fusion. (A) OCR. (B) Changes in proton leak and ATP production in mitochondrial respiration. (C) Changes in basal respiration and spare respiratory capacity in mitochondrial respiration. (D) Glycolysis stress test. (E) Parameters of glycolytic function. (F) Mitochondrial mass was estimated by ratio of mtDNA to gDNA. (G) Representative transmission electron microscopy images of mitochondria. Magnification: 500x. Arrows indicate elongated mitochondria. (H) Representative western blotting of mitochondrial fusion proteins OPA1, MFN1 and MFN2. (I) ROS concentration. *P<0.05, **P<0.01, ***P<0.001. ns, not significant; OCR, oxygen consumption rate; ECAR, extracelluar acidification rate; SUCLG1, succinate-CoA ligase GDP/ADP-forming subunit α; ROS, reactive oxygen species; mtDNA, mitochondrial DNA; OPA, Optic Atrophy Protein ; MFN, mitochondrial fusion protein; sh, short hairpin; NC, negative control; FCCP, trifluoromethoxy carbonylcyanide phenylhydrazone; DG, deoxy-glucose; OE, overexpression.

NC, cells in the OE-SUCLG1 had higher levels of mitochondrial fusion proteins (MFN1 and 2 and OPA1; Fig. 4H-K). Therefore, ROS measurement was performed to evaluate mitochondrial damage. The intracellular ROS levels were lower in the OE-SUCLG1, indicating reduced damage, but higher in shSUCLG1, indicating increased damage (Fig. 4L).

Effect of SUCLG1 expression on SLC25A1. Proteomics and metabolomics showed that in addition to SUCLG1, expression of CA was also affected in the TCA pathway (Table SIII). Thus, proteins that were associated with CA (CS, ACLY and SLC25A1) were investigated. Based on the WB results, SLC25A1 expression was increased when SUCLG1 expression was increased, and when SUCLG1 expression was decreased, then SLC25A1 was similarly decreased, whereas ACLY and CS were not affected by changes in SUCLG1 (Fig. 5A-D). Enzymatic activity assays also indicated no significant changes in the activities of the latter two proteins (Fig. 5E and F). For SLC25A1, partial functional recovery was observed. Compared with the OE-SUCLG1, cell function was inhibited in the OE-SUCLG1 inhibitor group (Fig. 5G-M). Cells in the OE group exhibited higher proliferation and wound healing rates (Fig. 5G-I). However, after adding the inhibitor, these abilities decreased but did not return to baseline, indicating that the function was only partially restored. The proportion of cells in S phase was significantly lower in cells with the addition of the inhibitor than in OE group but did not return to baseline (Fig. 5J and K). Apoptosis was also partially restored by the inhibitor (Fig. 5L and M).

Discussion

PNF, a common clinical manifestation of the rare genetic disorder NFI (17,18), develops in ~1/3 of patients (3). Although it is a benign tumor, there is a risk of transformation into MPNST, which occurs at the highest risk in childhood and adolescence and has a poor prognosis (19,20). A total of 8-13% of PNFs are at risk of developing Malignant Peripheral Nerve Sheath Tumor (21). Conventional radiotherapy is ineffective for PNF and surgery remains the only potentially effective treatment (6). In April 2020, the U.S. Food and Drug Administration approved the use of simetinib for pediatric patients aged ≥3 years for the treatment of inoperable symptomatic and/or progressive PNF; this provides symptomatic relief and tumor shrinkage in certain patients, but the drug remains ineffective in some patients, and the disease continues to progress (22,23). Although other MEK inhibitors have entered clinical trials (24-29), the role of metabolic changes in the disease is not yet known.

SUCLG1 is the α-subunit encoding the heterodimerization enzyme succinate coenzyme A ligase (30); previous studies (9,10) did not find the gene to be associated with tumors, but its mutation was associated with mitochondrial DNA depletion syndrome (11). However, a recent study by Yan *et al* (12), found that SUCLG1 restricts Polymerase (RNA) Mitochondrial (DNA Directed) succinylation to enhance mitochondrial biogenesis and leukemia progression. This suggests a potential association between SUCLG1 and tumors but to the best of our knowledge, this has been little studied (10-12). Here, SUCLG1 expression was upregulated in PNF, indicated by tissue mass spectrometry, and its expression was confirmed in tissue and cells. *In vitro* experiments showed that SUCLG1 promoted tumor cell proliferation and migration, inhibited apoptosis and affected the cell cycle, with an increased proportion of cells in S phase when expression is elevated.

The present mass spectrometry and metabolic analyses revealed that high expression of SUCLG1 and CA occurs in the TCA cycle pathway. The TCA cycle occurs in mitochondria; dysfunctional mitochondrial quality control is associated with development of numerous types of diseases, including tumors (31). Mitochondrial quality control involves numerous mechanisms that are largely dependent on the extent of mitochondrial damage, activating appropriate repair pathways (32). In this process, cells implement quality control through mitochondrial fusion and fission (33-35). SUCLG1 is a regulatory factor acting on mitochondria and previous studies (12,30) have revealed that it has a positive regulatory effect on mitochondrial quality, which was further validated in the present study (12). When the expression of SUCLG1 increased, there was an increase in the ratio of mitochondrial DNA to total genomic DNA and mitochondrial mass and fusion. ROS production was effectively suppressed, potentially because mitochondrial fusion decreased the degree of mitochondrial damage (36,37). These results suggested that in PNF cells, SUCLG1 exerts a key influence on mitochondrial quality control and promotes mitochondrial fusion.

The Warburg effect-where cells produce energy through aerobic glycolysis in the presence of sufficient oxygen and with intact mitochondrial function-is a key factor in driving cancer progression, leading to resistance to conventional therapy and poor patient prognosis (38,39). In certain tumor cases, mitochondrial defects, due to certain mutations in TCA cycle enzymes and overproduction of mitochondrial ROS, serve a key role in promoting the Warburg effect and tumor progression (38). By contrast, testing mitochondrial and glycolytic stress here demonstrated that SUCLG1, when expressed at elevated levels, primarily promoted mitochondrial respiratory capacity, with little effect on glycolytic processes. This result is different from previous results (38-40), which may be because the Warburg effect has been studied primarily in cancer and the tumors in the present study were benign and did not develop as fast as malignant tumors, therefore not requiring the Warburg effect to promote tumor development. It is possible that when PNFs are transformed into MPNATs, the Warburg pathway is initiated, providing a favorable microenvironment for malignant tumor progression. Here, more undamaged mitochondria provided sufficient energy for PNF cells. However, to demonstrate the promotion of tumor progression through SUCLG1 via aerobic respiration, further experiments is still needed.

When SUCLG1 levels increased, levels of metabolite CA, which is involved in the TCA cycle, were elevated. Key enzymes affecting its content, CS, ACLY and SLC25A1, may be directly responsible for this phenomenon. The first two enzymes are key enzymes in the TCA cycle and their expression was here unaffected. While SLC25A1 is a transporter protein on the mitochondrial membrane, SUCLG1 increased the mitochondrial mass, so it is likely that expression of SLC25A1 protein increased as well. Metabolite assay also revealed that the expression of CA increased with elevated expression of

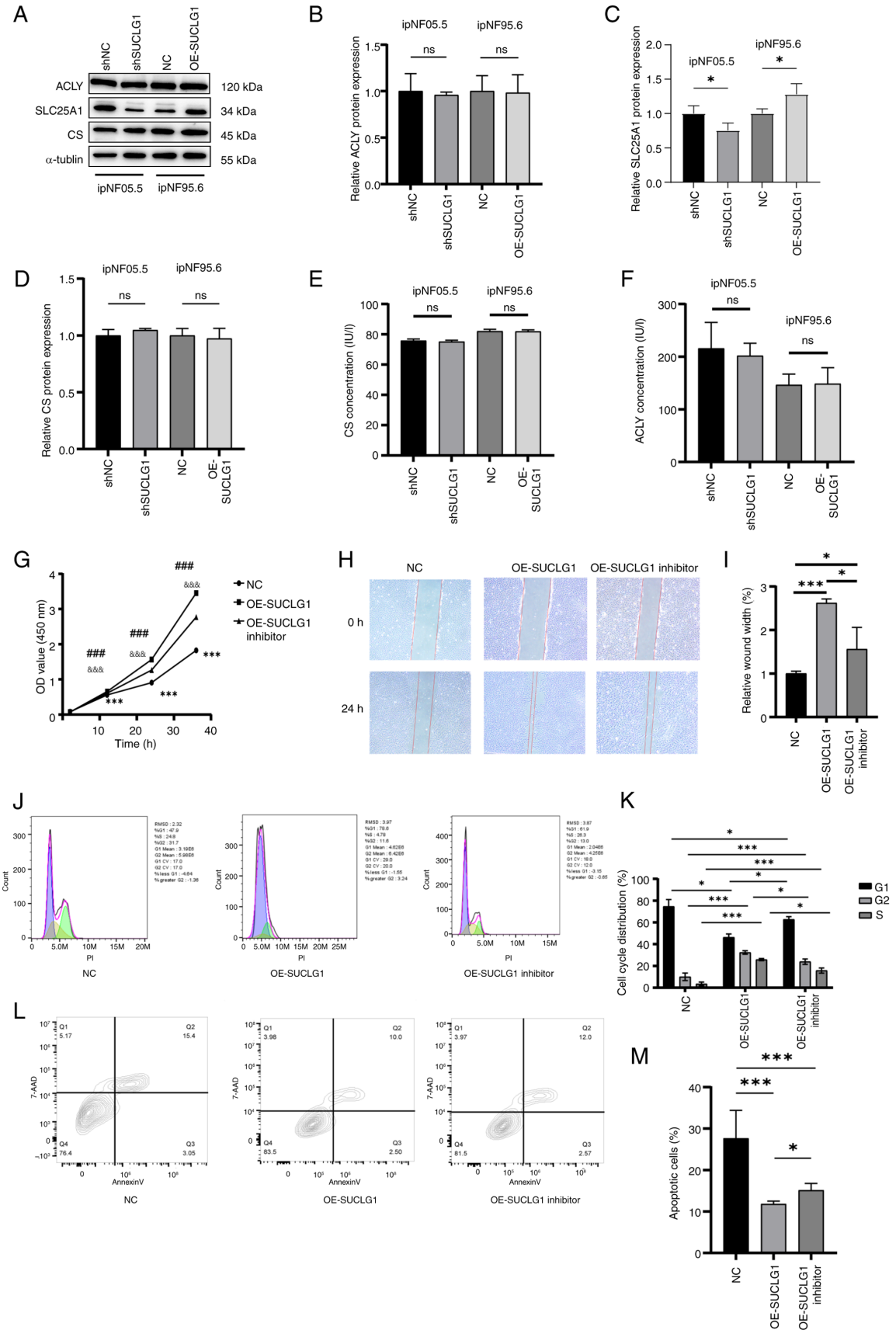

Figure 5. Effect of SUCLG1 expression on SLC25A1. (A) Representative Western blotting for (B) ACLY, (C) SLC25A1 and (D) CS. ELISA determination of (E) CS and (F) ACLY protein activity. (G) Cell proliferation was evaluated by the Cell Counting Kit-8 assay. (H) Wound healing assay. Magnification, x100. (I) Wound width of ipNF95.6 after transfection with NC and OE-SUCLG1 viruses and addition of SLC25A1 inhibitor. (J) Flow cytometry of (K) cell cycle distribution following transfection with NC and OE-SUCLG1 viruses and adding SLC25A1 inhibitor. (L) Flow cytometry of (M) apoptosis following transfection and adding SLC25A1 inhibitor. $^{\&\&\&}$P<0.001 vs. OE-SUCLG1 inhibitor. ***P<0.001 vs. NC, $^{\#\#\#}$P<0.001 vs. OE-SUCLG1, *P<0.05 vs. NC. SUCLG1, succinate-CoA ligase GDP/ADP-forming subunit α; ns, no significance; OD, optical density; SLC25A1, ;Solute Carrier Family 25 Member 1; ACLY, ATP Citrate Lyase; CS, Citrate Synthase; NC, negative control; OE, overexpression; sh, short hairpin.

SLC25A1. Thus, it was demonstrated that SUCLG1 affected CA expression by regulating SLC25A1 expression. Following addition of an inhibitor of SLC25A1 to cells overexpressing SUCLG1, function of PNF cells was partially restored, demonstrating that SUCLG1 affected the development of PNF cells via SLC25A1.

In vitro experiments proved that SUCLG1 served a key role in the progression of PNF and promoted aerobic respiration metabolism, but this needs to be verified *in vivo*. The present results not only provide a new potential target for the treatment of PNF, but also lay a preliminary foundation for further study of metabolic mechanisms.

Acknowledgements

Not applicable.

Funding

The present study was supported by National Natural Science Foundation of China (grant no. 82172227).

Availability of data and materials

The datasets generated and/or analyzed during the current study are not publicly available due to ongoing study but may be requested from the corresponding author.

Authors' contributions

QL and RH confirm the authenticity of all the raw data. ZZ conducted the experiments and analyzed the data. RH, QL and ZZ designed the study. RH and QL supervised the study. ZZ wrote the manuscript. All authors have read and approved the final manuscript.

Ethics approval and consent to participate

The present study was approved by Committee for Ethical Review of Research involving Human Subjects of Shandong Provincial Hospital, Jinan, China (approval no. SWYX2024-556). All human specimens were collected with informed written consent.

Patient consent for publication

Not applicable.

Competing interests

The authors declare that they have no competing interests.

References

1. Miller DT, Freedenberg D, Schorry E, Ullrich NJ, Viskochil D and Korf BR; Council on Genetics and American College of Medical Genetics and Genomics: Health supervision for children with neurofibromatosis type 1. Pediatrics 143: e20190660, 2019.
2. Acar S, Armstrong AE and Hirbe AC: Plexiform neurofibroma: Shedding light on the investigational agents in clinical trials. Expert Opin Investig Drugs 31: 31-40, 2021.
3. Fisher MJ, Blakeley JO, Weiss BD, Dombi E, Ahlawat S, Akshintala S, Belzberg AJ, Bornhorst M, Bredella MA, Cai W, *et al*: Management of neurofibromatosis type 1-associated plexiform neurofibromas. Neuro Oncol 24: 1827-1844, 2022.
4. Gross AM, Glassberg B, Wolters PL, Dombi E, Baldwin A, Fisher MJ, Kim A, Bornhorst M, Weiss BD, Blakeley JO, *et al*: Selumetinib in children with neurofibromatosis type 1 and asymptomatic inoperable plexiform neurofibroma at risk for developing tumor-related morbidity. Neuro Oncol 24: 1978-1988, 2022.
5. Zhu B, Zheng T, Wang W, Gu Y, Wei C, Li Q and Wang Z: Genotype-phenotype correlations of neurofibromatosis type 1: A cross-sectional study from a large Chinese cohort. J Neurol 271: 1893-1900, 2024.
6. Zhu B, Wei C, Wang W, Gu B, Li Q and Wang Z: Treatment and progress of cutaneous neurofibroma. Zhongguo Xiu Fu Chong Jian Wai Ke Za Zhi 36: 1064-1071, 2022 (In Chinese).
7. Dombi E, Baldwin A, Marcus LJ, Fisher MJ, Weiss B, Kim A, Whitcomb P, Martin S, Aschbacher-Smith LE, Rizvi TA, *et al*: Activity of selumetinib in neurofibromatosis type 1-related plexiform neurofibromas. N Engl J Med 375: 2550-2560, 2016.
8. Gross AM, Wolters PL, Dombi E, Baldwin A, Whitcomb P, Fisher MJ, Weiss B, Kim A, Bornhorst M, Shah AC, *et al*: Selumetinib in children with inoperable plexiform neurofibromas. N Engl J Med 382: 1430-1442, 2020.
9. Eniafe J and Jiang S: The functional roles of TCA cycle metabolites in cancer. Oncogene 40: 3351-3363, 2021.
10. Chen YM, Chen W, Xu Y, Lu CS, Zhu MM, Sun RY, Wang Y, Chen Y, Shi J and Wang D: Novel compound heterozygous SUCLG1 variants may contribute to mitochondria DNA depletion syndrome-9. Mol Genet Genomic Med 10: e2010, 2022.
11. Ramsheh S, Omidvar ME, Tabasinezhad M, Alipoor B, Salmani TA and Ghaedi H: SUCLG1 mutations and mitochondrial encephalomyopathy: A case study and review of the literature. Mol Biol Rep 47: 9699-9714, 2020.
12. Yan W, Xie C, Sun S, Zheng Q, Wang J, Wang Z, Man CH, Wang H, Yang Y, Wang T, *et al*: SUCLG1 restricts POLRMT succinylation to enhance mitochondrial biogenesis and leukemia progression. EMBO J 43: 2337-2367, 2024.
13. Icard P, Simula L, Zahn G, Alifano M and Mycielska ME: The dual role of citrate in cancer. Biochim Biophys Acta Rev Cancer 1878: 188987, 2023.
14. Arnold PK, Jackson BT, Paras KI, Brunner JS, Hart ML, Newsom OJ, Alibeckoff SP, Endress J, Drill E, Sullivan LB and Finley LWS: A non-canonical tricarboxylic acid cycle underlies cellular identity. Nature 603: 477-481, 2022.
15. Schmittgen TD and Livak KJ: Analyzing real-time PCR data by the comparative C(T) method. Nat Protoc 3: 1101-1108, 2008.
16. Thoudam T, Chanda D, Sinam IS, Kim BG, Kim MJ, Oh CJ, Lee JY, Kim MJ, Park SY, Lee SY, *et al*: Noncanonical PDK4 action alters mitochondrial dynamics to affect the cellular respiratory status. Proc Natl Acad Sci USA 119: e2120157119, 2022.
17. Well L, Döbel K, Kluwe L, Bannas P, Farschtschi S, Adam G, Mautner VF and Salamon J: Genotype-phenotype correlation in neurofibromatosis type-1: NF1 whole gene deletions lead to high tumor-burden and increased tumor-growth. PLOS Genet 17: e1009517, 2021.
18. Bernier A, Larbrisseau A and Perreault S: Cafe-au-lait macules and neurofibromatosis type 1: A review of the literature. Pediatr Neurol 60: 24-29.e1, 2016.
19. Nicoli TK, Saat R, Tarkkanen J, Kinnunen I, Mäkitie AA and Jero J: Challenging management of plexiform schwannoma and plexiform neurofibroma. J Craniofac Surg 33: 803-808, 2022.
20. Avery RA, Katowitz JA, Fisher MJ, Heidary G, Dombi E, Packer RJ and Widemann BC; OPPN Working Group: Orbital/periorbital plexiform neurofibromn children with neurofibromatosis type 1: Multidisciplinary recommendations for care. Ophthalmology 124: 123-132, 2017.
21. Wang W, Gu Y, Zhu B, *et al*: Retrospective study of surgical treatment in 121 patients with head and neck plexiform neurofibromas. Chin J Plast Surg 35: 169-178, 2024.
22. Jackson S, Baker EH, Gross AM, Whitcomb P, Baldwin A, Derdak J, Tibery C, Desanto J, Carbonell A, Yohay K, *et al*: The MEK inhibitor selumetinib reduces spinal neurofibroma burden in patients with NF1 and plexiform neurofibromas. Neurooncol Adv 2: vdaa095, 2020.
23. Veres K, Bene J, Hadzsiev K, Garami M, Pálla S, Happle R, Medvecz M and Szalai ZZ: Superimposed mosaicism in the form of extremely extended segmental plexiform neurofibroma caused by a novel pathogenic variant in the NF1 gene. Int J Mol Sci 24: 12154, 2023.

24. Wang D, Ge L, Guo Z, Li Y, Zhu B, Wang W, Wei C, Li Q and Wang Z: Efficacy and safety of trametinib in neurofibromatosis type 1-associated plexiform neurofibroma and low-grade glioma: A systematic review and meta-analysis. Pharmaceuticals (Basel) 15: 956, 2022.
25. Armstrong AE, Belzberg AJ, Crawford JR, Hirbe AC and Wang ZJ: Treatment decisions and the use of MEK inhibitors for children with neurofibromatosis type 1-related plexiform neurofibromas. BMC Cancer 23: 553, 2023.
26. Weiss BD, Wolters PL, Plotkin SR, Widemann BC, Tonsgard JH, Blakeley J, Allen JC, Schorry E, Korf B, Robison NJ, *et al*: NF106: A neurofibromatosis clinical trials consortium Phase II trial of the MEK inhibitor Mirdametinib (PD-0325901) in adolescents and adults with NF1-related plexiform neurofibromas. J Clin Oncol 39: 797-806, 2021.
27. Rizzo D, Ruggiero A, Amato M, Maurizi P and Riccardi R: BRAF and MEK inhibitors in pediatric glioma: New therapeutic strategies, new toxicities. Expert Opin Drug Metab Toxicol 12: 1397-1405, 2016.
28. Fisher MJ, Shih CS, Rhodes SD, Armstrong AE, Wolters PL, Dombi E, Zhang C, Angus SP, Johnson GL, Packer RJ, *et al*: Cabozantinib for neurofibromatosis type 1-related plexiform neurofibromas: A phase 2 trial. Nat Med 27: 165-173, 2021.
29. Gross AM, Glassberg B, Wolters PL, Dombi E, Baldwin A, Fisher MJ, Kim A, Bornhorst M, Weiss BD, Blakeley JO, *et al*: Selumetinib in children with neurofibromatosis type 1 and asymptomatic inoperable plexiform neurofibroma at risk for developing tumor-related morbidity. Neuro Oncol 24: 1978-1988, 2022.
30. Chinopoulos C, Batzios S, van den Heuvel LP, Rodenburg R, Smeets R, Waterham HR, Turkenburg M, Ruiter JP, Wanders RJA, Doczi J, *et al*: Mutated SUCLG1 causes mislocalization of SUCLG2 protein, morphological alterations of mitochondria and an early-onset severe neurometabolic disorder. Mol Genet Metab 126: 43-52, 2019.
31. Ho GT and Theiss AL: Mitochondria and inflammatory bowel diseases: Toward a stratified therapeutic intervention. Annu Rev Physiol 84: 435-459, 2022.
32. Sugiura A, Mclelland GL, Fon EA and Mcbride HM: A new pathway for mitochondrial quality control: Mitochondrial-derived vesicles. EMBO J 33: 2142-2156, 2014.
33. Zhang Z, Li TE, Chen M, Xu D, Zhu Y, Hu BY, Lin ZF, Pan JJ, Wang X, Wu C, *et al*: MFN1-dependent alteration of mitochondrial dynamics drives hepatocellular carcinoma metastasis by glucose metabolic reprogramming. Br J Cancer 122: 209-220, 2020.
34. You MH, Jeon MJ, Kim SR, Lee WK, Cheng SY, Jang G, Kim TY, Kim WB, Shong YK and Kim WG: Mitofusin-2 modulates the epithelial to mesenchymal transition in thyroid cancer progression. Sci Rep 11: 2054, 2021.
35. Wang Y, Wang Y, Liu W, Ding L, Zhang X, Wang B, Tong Z, Yue X, Li C, Xu L, *et al*: TIM-4 orchestrates mitochondrial homeostasis to promote lung cancer progression via ANXA2/PI3K/AKT/OPA1 axis. Cell Death Dis 14: 141, 2023.
36. Roca-Portoles A and Tait SWG: Mitochondrial quality control: From molecule to organelle. Cell Mol Life Sci 78: 3853-3866, 2021.
37. Yao CH, Wang R, Wang Y, Kung CP, Weber JD and Patti GJ: Mitochondrial fusion supports increased oxidative phosphorylation during cell proliferation. ELife 8: e41351, 2019.
38. Vaupel P and Multhoff G: Revisiting the Warburg effect: Historical dogma versus current understanding. J Physiol 599: 1745-1757, 2021.
39. Wang Y and Patti GJ: The Warburg effect: A signature of mitochondrial overload. Trends Cell Biol 33: 1014-1020, 2023.
40. Zhong X, He X, Wang Y, Hu Z, Huang H, Zhao S, Wei P and Li D: Warburg effect in colorectal cancer: The emerging roles in tumor microenvironment and therapeutic implications. J Hematol Oncol 15: 160, 2022.